

Holographic QCD phase diagram with critical point from Einstein-Maxwell-dilaton dynamics

J. Knaute, R. Yaresko, B. Kämpfer

*Helmholtz-Zentrum Dresden-Rossendorf, POB 51 01 19, 01314 Dresden, Germany and
TU Dresden, Institut für Theoretische Physik, 01062 Dresden, Germany*

Abstract

Supplementing the holographic Einstein-Maxwell-dilaton model of [1, 2] by input of lattice QCD data for 2+1 flavors and physical quark masses for the equation of state and quark number susceptibility at zero baryo-chemical potential we explore the resulting phase diagram over the temperature-chemical potential plane. A first-order phase transition sets in at a temperature of about 112 MeV and a baryo-chemical potential of 989 MeV. We estimate the accuracy of the critical point position in the order of approximately 5 % by considering different low-temperature asymptotics for the second-order quark number susceptibility. The critical pressure as a function of the temperature has a positive slope, i.e. the entropy per baryon jumps up when crossing the phase border line from larger values of temperature/baryo-chemical potential, thus classifying the phase transition as a gas-liquid one. The updated holographic model exhibits in- and outgoing isentropes in the vicinity of the first-order phase transition.

Keywords: gravity dual, holography, quark-gluon plasma, critical point
PACS: 11.25.Tq, 47.17.+e, 05.70.Ce, 12.38.Mh, 21.65.Mn

1. Introduction

The QCD phase diagram exhibits potentially a large variety of structures [3–6]. Either originating from extrapolations of weak-coupling results or being suggested by models (most notably Nambu–Jona-Lasinio (cf. [7]), linear sigma/quark-meson [8] models in numerous variants), various phases of

Email address: `j.knaute@hzdr.de` (J. Knaute)

strongly interacting matter may occur, such as color superconductors (cf. [9–11]), or quarkyonic matter (cf. [12]), or chirally restored phases (cf. [13]), or color-flavor locked structures (cf. [14]).

While the gas-liquid (GL) first-order phase transition (FOPT) in nuclear matter seems to be well established since some time [15–20], the hadron-quark (HQ) deconfinement transition still offers a few challenges. At very small or zero net-baryon density corresponding to a small chemical potential (μ)-to-temperature (T) ratio, $\mu/T \ll 1$, the HQ transition is established as a crossover in 2+1 flavor QCD with physical quark masses [21, 22] at a characteristic scale of $T_c = \mathcal{O}(150 \text{ MeV})$. The popular Columbia plot [23] sketches qualitatively the options of the phase structure in dependence of the u, d, s quark masses $m_{u,d,s}$. For instance, in the chiral limit, $m_{u,d,s} \rightarrow 0$, or the opposite infinitely heavy quark-mass limit, $m_{u,d,s} \rightarrow \infty$, the deconfinement transition is a FOPT. Due to the sign problem of the fermionic determinant the ab initio lattice QCD evaluations are not yet conclusive with respect to the confinement and chiral restoration transition(s) at non-zero baryochemical potential, in particular for $\mu/T > 2$. Some methods try to avoid or circumvent the sign problem (cf. [24]), e.g. by evaluations at imaginary μ (which need a prescription of $i\mu \rightarrow \mu$) or a Taylor expansion in powers of μ/T with coefficients calculated at $\mu = 0$ (which needs statements on the convergence [25]), or the reweighting method (which needs statements on the density and parameter ranges to incorporate the sign and overlap problem [26]).

The pertinent uncertainties make the region of larger μ/T interesting. A particularly interesting option is the possibility of a (critical) end point (CEP) of a curve of FOPTs, e.g. $T_c(\mu)$, setting in at (T_{CEP}, μ_{CEP}) and running toward the $T = 0$ axis when imaging the phase diagram in the $T - \mu$ plane. The CEP coordinates are yet fairly unconstrained. Plugging model results and QCD-related extrapolations together one arrives at some less conclusive scatter plot (cf. e.g. [24]). Advanced lattice QCD approaches disfavor a CEP position at $T/T_c(\mu = 0) > 0.9$ and $\mu/T \leq 2$ [25].

Experimentally, there are dedicated programs aiming at pinning down the CEP location. For instance, the beam energy scan at RHIC [27] gave hints on some features in the beam energy dependence of selected observables which have been interpreted as CEP signature (cf. [28]). In [29] another view has been launched with the conclusion of having also seen CEP indications. Furthermore, the SHINE (NA61) collaboration at CERN-SPS is also systematically seeking CEP effects [30]. Experiments planned at FAIR and

NICA and J-PARC [31] are analogously driven by CEP searches, analogously as goals by the CBM collaboration [32, 33], and the MPD group [34].

Given that challenges from both theory and experiment one can ask whether further theoretical model classes beyond the above mentioned approaches could be useful in exploring the hypothetical FOPT emerging from a CEP. Holographic models, advancing the seminal AdS/CFT correspondence [35–37], are thought to mimick essential QCD properties in the strong-coupling regime [38–42] and thus may serve as suitable candidates for such an enterprise. In [1, 2] a model formulation has been put forward which displays a critical point in the $T-\mu$ plane. While [1, 2] focuses on CEP properties and an outline of some transport coefficients, [43, 44] employed that holographic model to investigate thermodynamics and further transport quantities at small μ/T , however, the question of the CEP position, based on an adjustment to recent lattice data, and properties of phase diagrams were not addressed. The model rests on the coupled Einstein-Maxwell-dilaton (EMd) dynamics and can be adjusted to QCD thermodynamics, i.e. the equation of state (EoS) and quark number susceptibility at $\mu = 0$. The resulting phase structure is the topic of our present paper. We feel that an update of [1, 2] is timely since by now consistent and more precise lattice QCD data are at our disposal. In fact, we find some some qualitatively important modifications in comparison to [1, 2] w.r.t. the pattern of isentropes in the phase diagrams as well as the position of the CEP.

With respect to the discussion in [45], a FOPT curve is specified by further peculiarities: it can be related either to a GL type or to a HQ type transition. For a discussion contrasting features of GL and HQ phase transitions we refer the interested reader to [45–48], where the notions of entropic vs. enthalpic transitions as well as congruent and non-congruent material changes are exemplified and representations in other variables than $T-\mu$ are exhibited. Such different FOPTs can matter significantly in core-collapse supernova explosions as discussed in some detail in [49]. Motivated by such a relation to astrophysical aspects of the phase structure of strongly interacting matter - not only touching core-collapse dynamics but also neutron (quark core) stars - we unravel here the phase structure of the holographic EMd model. It turns out that the EMd model with adjustments to QCD input belongs to the GL class. That is across the phase boundary both the baryon density n and the entropy density s jump when considering the stable phases. For the GL transition, the entropy per baryon s/n drops down when going into μ or T direction, while at the HQ transition s/n jumps up, according to ex-

pectations in [45]. According to the Clausius-Clapeyron equation one finds the critical pressure $p(T, \mu_c(T))$ either with positive slope (GL transition) or with negative slope (HQ transition).¹

Our paper is organized as follows. In section 2 we recall the holographic EMd model. The numerical adjustment to lattice QCD data at $\mu = 0$ is described in section 3 and the numerical results for the phase diagrams are presented in section 4, including an analysis of the impact of different assumptions for the susceptibility at small temperatures. We summarize in section 5.

2. Recalling the holographic EMd model

The holographic model of gravity of a 5-dimensional Riemann space sourced by the coupled Maxwell-dilaton fields is defined in [1, 2] by the action

$$S = \frac{1}{2\kappa_5^2} \int d^5x \sqrt{-g} \left(R - \frac{1}{2} \partial^\mu \phi \partial_\mu \phi - V(\phi) - \frac{f(\phi)}{4} F_{\mu\nu}^2 \right) + S_{GH}, \quad (1)$$

where R is the Einstein-Hilbert part, $F_{\mu\nu} = \partial_\mu A_\nu - \partial_\nu A_\mu$ with $A_\mu dx^\mu = \Phi dt$ stands for the Abelian gauge field à la Maxwell, and ϕ is a real scalar (dilaton) with self-interaction described by the so called potential $V(\phi)$. The Maxwell field and dilaton are coupled by a dynamical strength function $f(\phi)$. The Gibbons-Hawking term S_{GH} for a consistent formulation of the variational problem is not needed explicitly in our context. The “Einstein constant” κ_5 is taken as a model parameter. The ansatz for the infinitesimal line element squared

$$ds^2 = e^{2A(r;r_H)} \left(-h(r;r_H) dt^2 + d\vec{x}^2 \right) + \frac{e^{2B} dr^2}{h(r;r_H)} \quad (2)$$

highlights that (i) only the dynamics in bulk direction r is considered and (ii) a horizon is admitted at $r = r_H$ by a simple zero of the blackness function h . By a gauge choice, one can achieve $B = 0$ and $r_H = 0$. We solve the field equations following from (1, 2) with the technique described in [1, 2]. In a nutshell: One has to numerically integrate from $r_H + \epsilon$ towards the boundary

¹Obviously, the resulting behavior of the pressure at the FOPT at smaller temperatures is markedly depending on these details, with impact on the stiffness of the EoS which in turn governs the possibility of a third family of compact stars or twin configurations [50–53], on which the options for core-collapse supernova explosions according to [49] (and further references therein) depend on.

at $r \rightarrow \infty$. Requiring regularity of A, h, ϕ, Φ at the horizon $r = r_H$, defined by $h(r_H; r_H) = 0$, series solutions for any these functions can be obtained, which yield the initial conditions for the integration. After fixing all gauge redundancies the two remaining independent quantities parametrizing the solutions are $\phi_0 \equiv \phi(r_H, r_H)$ and $\Phi_1 \equiv \frac{\partial \Phi}{\partial r} \big|_{r_H}$. It follows from the horizon expansion of A that Φ_1 is bounded, $\Phi_1 < \Phi_1^{\max} \equiv \sqrt{-\frac{2V(\phi_0)}{f(\phi_0)}}$. Close to the boundary, the following expansions in powers of $e^{-\alpha(r)} \equiv \exp[-\frac{r}{L\sqrt{h_0^\infty}} - A_0^\infty]$ are valid: $h(r) = h_0^\infty + \dots$, $A(r) = a(r) + \dots$, $\Phi(r) = \Phi_0^\infty + \Phi_2^\infty e^{-2\alpha(r)} + \dots$, and $\phi(r) = \phi_A e^{-(4-\Delta)\alpha(r)} + \phi_B e^{-\Delta\alpha(r)} + \dots$. The expansion of ϕ assumes $L^2 V(\phi) = -12 + \frac{1}{2}[\Delta(\Delta-4)]^2 \phi^2 + \dots$ for $\phi \rightarrow 0$.² By the standard AdS/CFT dictionary, ϕ_A is the source and ϕ_B the expectation value of the boundary theory operator dual to ϕ . Then one obtains the thermodynamic quantities temperature T , entropy density s , baryo-chemical potential μ and baryon density n as

$$T = \lambda_T \frac{1}{4\pi} \frac{1}{L\phi_A^{1/(4-\Delta)} \sqrt{h_0^\infty}}, \quad (3)$$

$$s = \lambda_s \frac{2\pi}{\kappa_5} \frac{1}{\phi_A^{3/(4-\Delta)}}, \quad (4)$$

$$\mu = \lambda_\mu 4\pi \Phi_0^\infty T, \quad (5)$$

$$n = \lambda_n \frac{LQ_G}{4\pi f(0)} s. \quad (6)$$

The dimensional scaling factors $\lambda_{T,s,\mu,n}$ are introduced to compensate the arbitrary interim choice $\kappa_5 = L = 1$ and restore physical units (here, L is the AdS scale). At the horizon, the radially conserved Gauss charge becomes $Q_G = f(\phi_0)\Phi_1$. In such a way one maps out the $T-\mu$ plane by suitably chosen pairs (ϕ_0, Φ_1) which entirely parameterise initial conditions at r_H ; (4) and (6) deliver in each point s and n . The pressure follows from the integration of $dp(T, \mu) = s(T, \mu)dT + n(T, \mu)d\mu$, with $p(0, 0) = 0$, where $T = 0, \mu = 0$ correspond to $\phi_0 \rightarrow \infty, \Phi_1 = 0$.

The given bottom-up approach is to be supplemented by fixing the dilaton

²This means we are considering a relevant operator in the boundary theory with scaling dimension $\Delta < 4$; see [54] for a different choice of potential asymptotics that correspond to a marginal operator.

potential $V(\phi)$ and the dynamical coupling $f(\phi)$, e.g. from lattice QCD results at $\mu = 0$. By properly engineering $V(\phi)$ one essentially dials the EoS at $\mu = 0$, in particular whether a FOPT is built in (as for pure glue dynamics or QCD in the chiral limit(s)) or a crossover is incorporated (as for 2+1 flavor QCD with physical quark masses), see [55, 56] for recent examples and [54, 57] for full-fledged pioneering investigations. Adjusting $f(\phi)$ at the quark number susceptibility from lattice QCD at $\mu = 0$ completes the model. Beyond $p - s - n$ thermodynamics also fluctuation measures, such as susceptibilities, variance, kurtosis, etc. follow via derivatives of the pressure. The susceptibilities are defined, in general, by $\chi_i(T, \mu) \equiv \frac{\partial^i p(T, \mu)}{\partial \mu^i} \Big|_T$, $i = 2, 3, 4, \dots$. By CP invariance, odd susceptibilities $\chi_{3, 5, \dots}$ at $\mu = 0$ vanish. In [1, 2], a comfortable formula for χ_2 at $\mu = 0$ is given (see also [43, 44])

$$\frac{\chi_2(T, 0)}{T^2} = \frac{L}{16\pi^2 f(0)} \frac{s}{T^3} \frac{1}{\int_{r_H}^{\infty} dr \frac{e^{-2A}}{f(\phi)}}, \quad (7)$$

which allows the matching of $f(\phi)$ to lattice data.

The EMd model (1, 2) with these input data is then ready to transport the information from $\mu = 0$ to $\mu > 0$, up to $T = 0$, thus uncovering the $T - \mu$ plane. This is very much the spirit of the quasi-particle model [58–60], where a flow equation facilitates such a transport.

3. Adjustment to lattice QCD data at $\mu = 0$

Contrary to [43, 44] we rely here on a modified previous fit [56] to the 2+1 flavor QCD thermodynamics with physical quark masses [21, 22] by the dilaton potential

$$V(\phi) = \begin{cases} -12 \exp\left(\frac{a_1}{2}\phi^2 + \frac{a_2}{4}\phi^4\right) & : \phi < \phi_m \\ a_{10} \cosh[a_4(\phi - a_5)]^{a_3/a_4} \exp\left\{a_6\phi + \frac{a_7}{a_8} \tanh[a_8(\phi - a_9)]\right\} & : \phi \geq \phi_m \end{cases} \quad (8)$$

with parameters

$$\begin{array}{c|c|c|c|c|c} \phi_m & a_1 & a_2 & a_3 & a_4 & a_5 \\ \hline 1.7058 & 0.2840 & -0.0089 & 0.7065 & 0.4951 & 0.1761 \\ \hline a_6 & a_7 & a_8 & a_9 & a_{10} \\ \hline -0.0113 & -0.4701 & 2.1420 & 4.3150 & -10.0138 \end{array}, \quad (9)$$

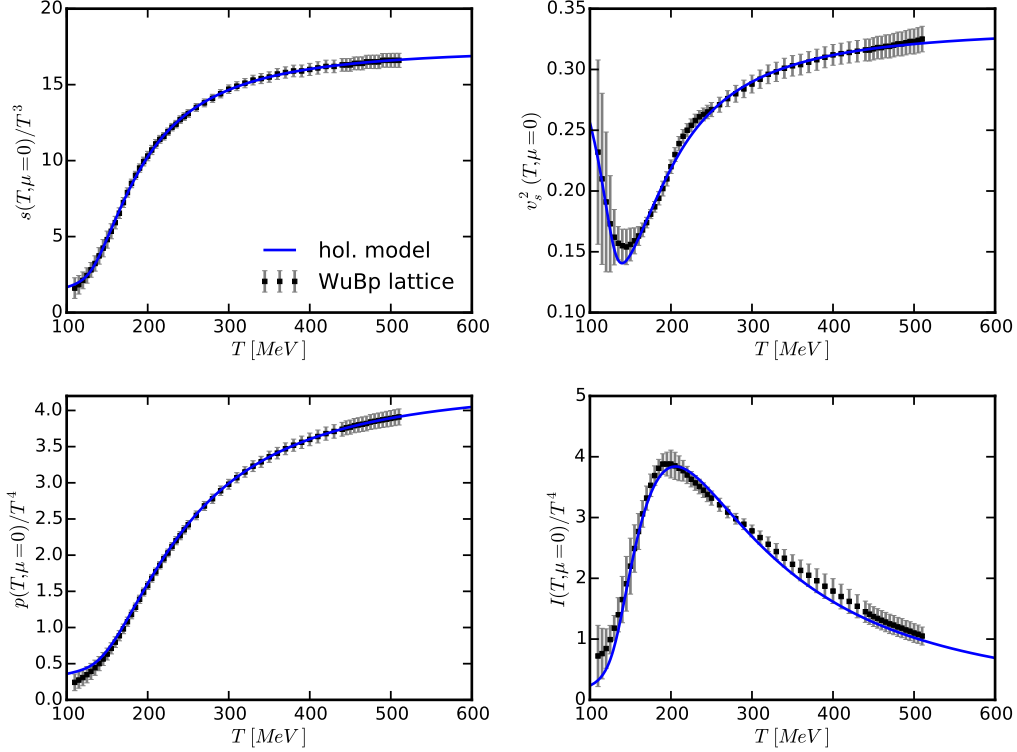


Figure 1: Equation of state of the updated holographic EMd model with parametrizations (8)-(12) as functions of T for $\mu = 0$: scaled entropy density (top left), speed of sound squared $v_s^2 = \frac{\partial \log T}{\partial \log s}$ (top right), scaled pressure (bottom left) and scaled trace anomaly (bottom right). Lattice results from [21] are displayed as symbols with error bars.

implying $\Delta = 2(1 + \sqrt{1 - 3a_1})$. A fit of χ_2/T^2 from [61] by the ansatz in (7)

$$f(\phi) = c_0 + c_1 \tanh [c_2(\phi - c_3)] \quad (10)$$

delivers the parameters

$$\begin{array}{c|c|c|c} c_0 & c_1 & c_2 & c_3 \\ \hline 0.1892 & -0.1659 & 1.5497 & 2.1820 \end{array} \quad (11)$$

together with the fit results

$$\begin{array}{c|c|c|c} \lambda_T & \lambda_s & \lambda_\mu & \lambda_n \\ \hline 1148 \text{ MeV} & (513 \text{ MeV})^3 & 1854 \text{ MeV} & (430 \text{ MeV})^3 \end{array} . \quad (12)$$

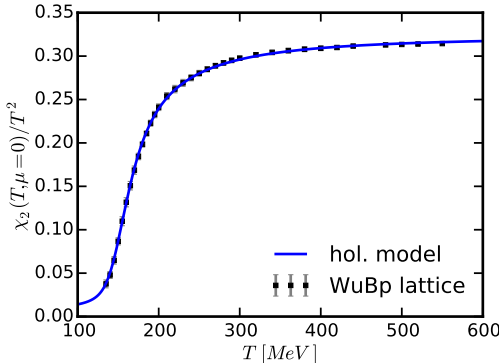


Figure 2: Second-order susceptibility χ_2/T^2 of the updated holographic EMd model with parametrizations (8)-(12) as function of T for $\mu = 0$. Lattice results from [61] are displayed as symbols with error bars.

Uncharged black hole solutions are numerically generated with initial conditions $\Phi_1 = 0$ and $\phi_0 \in [0.35, 5.0]$. The resulting equation of state for $\mu = 0$ is shown in Fig. 1 and the corresponding susceptibility is exhibited in Fig. 2. We emphasize the consistency of the lattice data in [21] and [22] and select the data of [21] for a comparison. The multi-parameter ansätze (8)-(12) allow in fact a fairly precise description of the available data.

4. Phase diagram

Charged black hole solutions with initial conditions $\phi_0 \in [0.5, 4.5]$ and $\Phi_1/\Phi_1^{max}(\phi_0) \in [0, 0.78]$ result in the thermodynamic phase diagram exhibited in Fig. 3 in various variants over the $T - \mu$ plane. Only the stable-phase quantities are shown, i.e. in the case of multi-valued solutions at a given $T - \mu$ point those with maximum pressure. The CEP coordinates are $T_{CEP} = (111.5 \pm 0.1)$ MeV and $\mu_{CEP} = (988.9 \pm 0.7)$ MeV. These uncertainties are estimated through the numerically non-unique intersection point of the spinodals and critical temperature curve.

The FOPT curve shows up as kinky behavior of the pressure and jumpy behavior of the entropy density, baryon density and entropy-to-baryon ratio (cf. corresponding panels in Fig. 3).

The contour curves in the pressure panel in Fig. 3 are scaled isobars, $p/T^4 = \text{const}$. The pressure increases in μ -direction (e.g. at constant T). The FOPT curve is steeper than neighboring isobars, as characteristic for the GL FOPT. This implies that the critical pressure $p_c(T) = p(T, \mu_c(T))$ increases with temperature, see right panel in Fig. 4. The information on both entropy

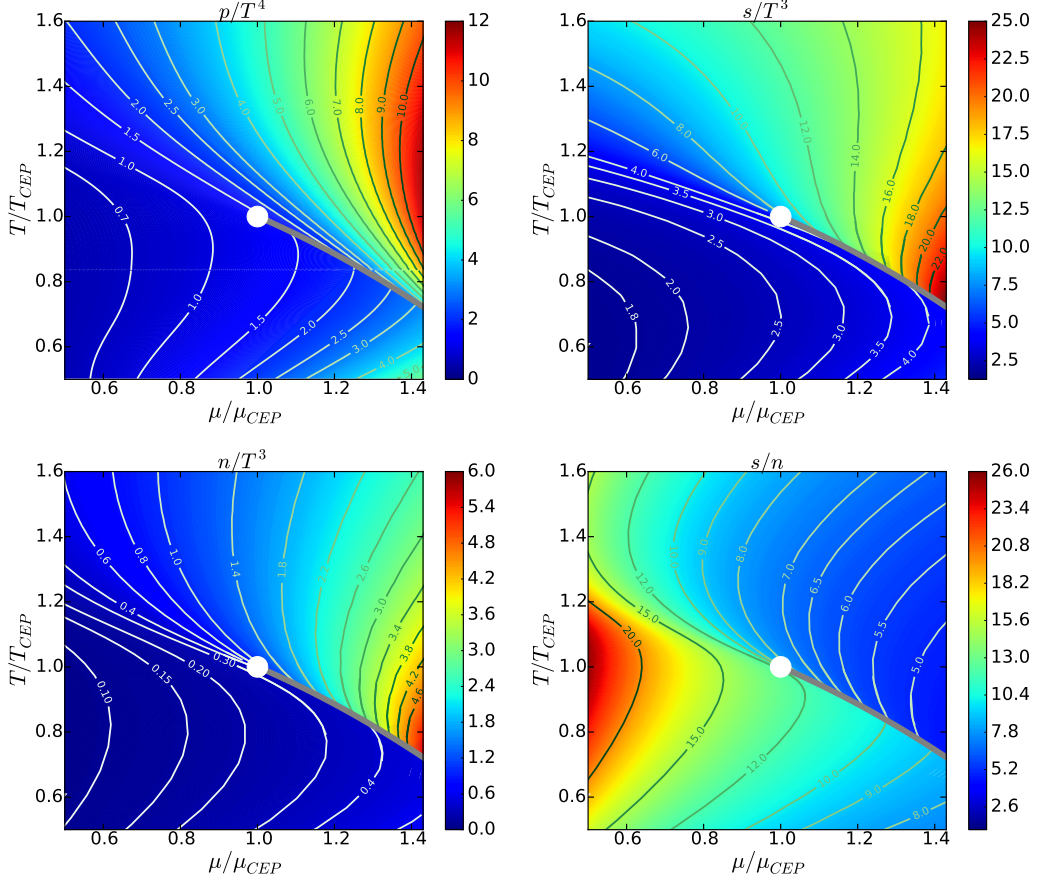


Figure 3: Contour plots of scaled pressure (top left), scaled entropy density (top right), scaled baryon density (bottom left), and entropy-to-baryon ratio (bottom right) over the scaled $T - \mu$ plane for the updated holographic EMD model. The position of the CEP is marked by a white dot and the FOPT curve is displayed as grey line.

density and baryon density (see top right and bottom left panel in Fig. 3) can be combined to the contour plot of constant entropy per baryon, see bottom right panel in Fig. 3. The resulting contour curves are isentropes, i.e. paths of gas or fluid elements during an adiabatic expansion (collapse) stage in heavy-ion collisions (stellar core collapse). The scaled pressure, entropy density and baryon density are pushed towards higher values with increasing chemical potential, whereas the entropy-to-baryon ratio is decreasing. For $\mu \geq \mu_{CEP}$ the scaled entropy density, scaled baryon density and entropy-to-

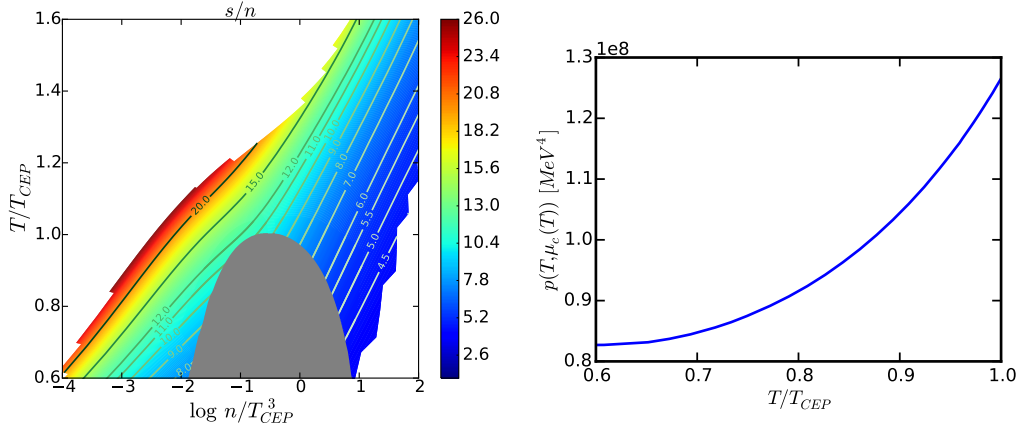


Figure 4: Left panel: Contour plots of entropy-to-baryon ratio over the T/T_{CEP} – $\log(n/T_{CEP}^3)$ plane for the updated holographic EMd model. The coexistence region is shown in grey. White regions indicate areas that are beyond the range displayed in the phase diagrams in Fig. 3. Right panel: Critical pressure $p_c = p(T, \mu_c(T))$ for the updated holographic EMd model.

baryon ratio jump across the FOPT.

Comparing the entropy-to-baryon ratios on both sides of a point on the FOPT curve evidences $s/n|_- > s/n|_+$, where the label $-(+)$ means approaching the FOPT curve from left (right). In line with the above mentioned Clausius-Clapeyron relation $dp_c(T)/dT = (\frac{s}{n}|_- - \frac{s}{n}|_+) (\frac{1}{n}|_- - \frac{1}{n}|_+)$, this implies in turn that the curve $p(T, \mu_c(T))$ as a function of T has positive slope, see Fig. 4 (right panel), as typical for the GL transition. Isentropes meeting the FOPT curve are “incoming” on the deconfined/dense (+) side and “outgoing” on the confined/dilute (–) side. Figure 4 (left panel) illustrates this behavior in the T – $\log n$ plane. The two-phase coexistence region is depicted by a grey region, where the isentropes (not displayed) are to be constructed by the lever rule. The panel exposes the shape of the isentropes as paths of adiabatically expanding and cooling pieces of matter: In the updated EMd model, isentropes enter *and* leave the coexistence region. This is in contrast to [1, 2] where only incoming isentropes can be found. According to the nomenclature of [48], the updated EMd model is classified as type IA and represents a GL phase transition.

The updated holographic EMd model is based on a fit to the recent lattice data for $\mu = 0$. Since no lattice results are available for low-temperatures

and the critical point is located in a temperature range where the lattice data just start, we estimate this uncertainty by assuming different generic low-temperature asymptotics for the second order quark number susceptibility. The different behaviors are realized by a modified parametrization of the gauge kinetic function $f(\phi)$ for low-temperatures. The different types (e.g. continuing the data exhibited in Fig. 2 straight ahead to zero or shifting the leveling off down) just slightly vary T_{CEP} in the order of 5 MeV and μ_{CEP} in the order of 50 MeV, corresponding to a relative uncertainty of approximately 5 % respectively.

5. Summary

In summary we explore here the phase structure of the holographic Einstein-Maxwell-dilaton (EMd) model [1, 2] adjusted now at $2 + 1$ flavor lattice QCD data with physical quark masses at $\mu = 0$. The EMd model has a first-order phase transition (FOPT) curve setting in at a (critical) endpoint (CEP) with coordinates $T_{CEP} = 112$ MeV, $\mu_{CEP} = 989$ MeV. By considering different low-temperature asymptotics for the second order quark number susceptibility and analyzing the resulting critical point locations, we estimate the relative uncertainty of our result for the critical point position in the order of approximately 5 %. We emphasize that these values are consistent with recent lattice estimates [25].

The FOPT curve continues from the CEP towards the $T = 0$ axis. Recalling the general remarks in [43, 44] we refrain from analysing the region of small temperatures (i.e. we leave the quantum phase transition for separate consideration), which however is relevant w.r.t. neutron (quark) stars and particular scenarios for core-collapse supernova explosions. The EMd model does not include explicitly such QCD relevant aspects as chiral symmetry or confinement. Instead, it accounts implicitly for these fundamental notions by the adjustment at QCD results.

The resulting phase diagram resembles in many aspects the gas-liquid phase transition. For instance, the critical pressure increases with temperature, contrary to expectations of the hadron-quark transition. In the updated EMd model, isentropes are incoming from the dense phase, enter the coexistence region, run through and leave the critical curve at lower temperature. The updated EMd model exhibits a graceful exit into the pure low-temperature and low-dense phase.

We emphasize the need to supplement (model) phase diagrams by information on isobars or isentropes, for instance, for having access to physics implications.

Acknowledgements: Enlightening conversations with J. Noronha on holographic models are gratefully acknowledged. We thank J. Randrup and V. Koch for discussions on phase transitions and S. Borsanyi for supplying data of susceptibilities shown in [61]. Options for the hadron-quark transition have been discussed with B. Friman some time ago.

References

- [1] O. DeWolfe, S. S. Gubser, and C. Rosen, Phys. Rev. **D 83**, 086005 (2011), arXiv:1012.1864 [hep-th]
- [2] O. DeWolfe, S. S. Gubser, and C. Rosen, Phys. Rev. **D 84**, 126014 (2011), arXiv:1108.2029 [hep-th]
- [3] K. Fukushima and C. Sasaki, Prog. Part. Nucl. Phys. **72**, 99 (2013), arXiv:1301.6377 [hep-ph]
- [4] H.-T. Ding, F. Karsch, and S. Mukherjee, Int. J. Mod. Phys. **E 24**, 1530007 (2015), arXiv:1504.05274 [hep-lat]
- [5] P. Braun-Munzinger, V. Koch, T. Schäfer, and J. Stachel, Phys. Rept. **621**, 76 (2016), arXiv:1510.00442 [nucl-th]
- [6] K. Fukushima and T. Kojo, Astrophys. J. **817**, 180 (2016), arXiv:1509.00356 [nucl-th]
- [7] I. F. Ranea-Sandoval, S. Han, M. G. Orsaria, G. A. Contrera, F. Weber, and M. G. Alford, Phys. Rev. **C 93**, 045812 (2016), arXiv:1512.09183 [nucl-th]
- [8] L. Olbrich, M. Zétényi, F. Giacosa, and D. H. Rischke, Phys. Rev. **D 93**, 034021 (2016), arXiv:1511.05035 [hep-ph]
- [9] T. Schäfer and F. Wilczek, Phys. Rev. **D 60**, 114033 (1999), arXiv:hep-ph/9906512 [hep-ph]

- [10] M. G. Alford, A. Schmitt, K. Rajagopal, and T. Schäfer, Rev. Mod. Phys. **80**, 1455 (2008), arXiv:0709.4635 [hep-ph]
- [11] R. Rapp, T. Schäfer, E. V. Shuryak, and M. Velkovsky, Phys. Rev. Lett. **81**, 53 (1998), arXiv:hep-ph/9711396 [hep-ph]
- [12] A. Andronic *et al.*, Nucl. Phys. **A 837**, 65 (2010), arXiv:0911.4806 [hep-ph]
- [13] J. Eser, M. Grahl, and D. H. Rischke, Phys. Rev. **D 92**, 096008 (2015), arXiv:1508.06928 [hep-ph]
- [14] D. Nickel, R. Alkofer, and J. Wambach, Phys. Rev. **D 74**, 114015 (2006), arXiv:hep-ph/0609198 [hep-ph]
- [15] J. E. Finn *et al.*, Phys. Rev. Lett. **49**, 1321 (1982)
- [16] R. W. Minich *et al.*, Phys. Lett. **B 118**, 458 (1982)
- [17] A. S. Hirsch, A. Bujak, J. E. Finn, L. J. Gutay, R. W. Minich, N. T. Porile, R. P. Scharenberg, B. C. Stringfellow, and F. Turkot, Phys. Rev. **C 29**, 508 (1984)
- [18] J. Pochodzalla *et al.*, Phys. Rev. Lett. **75**, 1040 (1995)
- [19] J. B. Natowitz, K. Hagel, Y. Ma, M. Murray, L. Qin, R. Wada, and J. Wang, Phys. Rev. Lett. **89**, 212701 (2002), arXiv:nucl-ex/0204015 [nucl-ex]
- [20] V. A. Karnaughov *et al.*, Phys. Rev. **C 67**, 011601 (2003), arXiv:nucl-ex/0302006 [nucl-ex]
- [21] S. Borsanyi, Z. Fodor, C. Hoelbling, S. D. Katz, S. Krieg, and K. K. Szabo, Phys. Lett. **B 730**, 99 (2014), arXiv:1309.5258 [hep-lat]
- [22] A. Bazavov *et al.* (HotQCD), Phys. Rev. **D 90**, 094503 (2014), arXiv:1407.6387 [hep-lat]
- [23] F. R. Brown, F. P. Butler, H. Chen, N. H. Christ, Z.-h. Dong, W. Schäfer, L. I. Unger, and A. Vaccarino, Phys. Rev. Lett. **65**, 2491 (1990)

- [24] M. A. Stephanov, *Proceedings, 24th International Symposium on Lattice Field Theory (Lattice 2006): Tucson, USA, July 23-28, 2006*, PoS **LAT2006**, 024 (2006), arXiv:hep-lat/0701002 [hep-lat]
- [25] A. Bazavov *et al.*, (2017), arXiv:1701.04325 [hep-lat]
- [26] R. Iwami, S. Ejiri, K. Kanaya, Y. Nakagawa, D. Yamamoto, and T. Umeda, Phys. Rev. **D 92**, 094507 (2015), arXiv:1508.01747 [hep-lat]
- [27] X. Luo (STAR), *Proceedings, 9th International Workshop on Critical Point and Onset of Deconfinement (CPOD 2014): Bielefeld, Germany, November 17-21, 2014*, PoS **CPOD2014**, 019 (2015), arXiv:1503.02558 [nucl-ex]
- [28] M. Mustafa (STAR), *Proceedings, 25th International Conference on Ultra-Relativistic Nucleus-Nucleus Collisions (Quark Matter 2015): Kobe, Japan, September 27-October 3, 2015*, Nucl. Phys. **A 956**, 43 (2016), arXiv:1512.09329 [nucl-ex]
- [29] R. A. Lacey, *Proceedings, 25th International Conference on Ultra-Relativistic Nucleus-Nucleus Collisions (Quark Matter 2015): Kobe, Japan, September 27-October 3, 2015*, Nucl. Phys. **A 956**, 348 (2016), arXiv:1512.09152 [nucl-ex]
- [30] E. Andronov (NA61/SHINE), *Proceedings, 4th International Conference on New Frontiers in Physics (ICNFP 2015): Kolymbari, Greece, August 23-30, 2015*, EPJ Web Conf. **126**, 04003 (2016), arXiv:1512.05938 [nucl-ex]
- [31] H. Sako *et al.*, *Proceedings, 24th International Conference on Ultra-Relativistic Nucleus-Nucleus Collisions (Quark Matter 2014): Darmstadt, Germany, May 19-24, 2014*, Nucl. Phys. **A 931**, 1158 (2014)
- [32] <http://www.fair-center.eu/for-users/experiments/cbm.html>
- [33] B. Friman, C. Hohne, J. Knoll, S. Leupold, J. Randrup, R. Rapp, and P. Senger, Lect. Notes Phys. **814**, pp.1 (2011)
- [34] A. Sorin, V. Kekelidze, A. Kovalenko, R. Lednicky, I. Meshkov, and G. Trubnikov, *Proceedings, 4th International Conference on Hard and Electromagnetic Probes of High-Energy Nuclear Collisions (Hard Probes 2010): Eilat, Israel, October 10-15, 2010*, Nucl. Phys. **A 855**, 510 (2011)

- [35] J. M. Maldacena, Int. J. Theor. Phys. **38**, 1113 (1999), [Adv. Theor. Math. Phys. 2, 231 (1998)], arXiv:hep-th/9711200 [hep-th]
- [36] S. S. Gubser, I. R. Klebanov, and A. M. Polyakov, Phys. Lett. **B 428**, 105 (1998), arXiv:hep-th/9802109 [hep-th]
- [37] E. Witten, Adv. Theor. Math. Phys. **2**, 253 (1998), arXiv:hep-th/9802150 [hep-th]
- [38] J. Casalderrey-Solana, H. Liu, D. Mateos, K. Rajagopal, and U. A. Wiedemann, (2011), 10.1017/CBO9781139136747, arXiv:1101.0618 [hep-th]
- [39] O. DeWolfe, S. S. Gubser, C. Rosen, and D. Teaney, Prog. Part. Nucl. Phys. **75**, 86 (2014), arXiv:1304.7794 [hep-th]
- [40] N. Brambilla *et al.*, Eur. Phys. J. **C 74**, 2981 (2014), arXiv:1404.3723 [hep-ph]
- [41] A. Adams, L. D. Carr, T. Schäfer, P. Steinberg, and J. E. Thomas, New J. Phys. **14**, 115009 (2012), arXiv:1205.5180 [hep-th]
- [42] T. Schäfer and D. Teaney, Rept. Prog. Phys. **72**, 126001 (2009), arXiv:0904.3107 [hep-ph]
- [43] R. Rougemont, A. Ficnar, S. Finazzo, and J. Noronha, JHEP **04**, 102 (2016), arXiv:1507.06556 [hep-th]
- [44] R. Rougemont, J. Noronha, and J. Noronha-Hostler, Phys. Rev. Lett. **115**, 202301 (2015), arXiv:1507.06972 [hep-ph]
- [45] J. Steinheimer, J. Randrup, and V. Koch, Phys. Rev. **C 89**, 034901 (2014), arXiv:1311.0999 [nucl-th]
- [46] M. Hempel, V. Dexheimer, S. Schramm, and I. Iosilevskiy (2015) arXiv:1512.07116 [nucl-th]
- [47] I. Iosilevskiy, in *Proceedings, Compact Stars in the QCD Phase Diagram IV (CSQCD IV): Prerow, Germany, September 26-30, 2014* (2015) arXiv:1504.05850 [nucl-th]

- [48] F. Wunderlich, R. Yaresko, and B. Kämpfer, *J. Mod. Phys.* **7**, 852 (2016), arXiv:1604.00179 [hep-ph]
- [49] M. Hempel, O. Heinemann, A. Yudin, I. Iosilevskiy, M. Liebendörfer, and F.-K. Thielemann, *Phys. Rev. D* **94**, 103001 (2016), arXiv:1511.06551 [nucl-th]
- [50] B. Kämpfer, *Phys. Lett. B* **153**, 121 (1985)
- [51] K. Schertler, C. Greiner, J. Schaffner-Bielich, and M. H. Thoma, *Nucl. Phys. A* **677**, 463 (2000), arXiv:astro-ph/0001467 [astro-ph]
- [52] M. G. Alford, G. F. Burgio, S. Han, G. Taranto, and D. Zappalà, *Phys. Rev. D* **92**, 083002 (2015), arXiv:1501.07902 [nucl-th]
- [53] D. Alvarez-Castillo, A. Ayriyan, S. Benic, D. Blaschke, H. Grigorian, and S. Typel, *Eur. Phys. J. A* **52**, 69 (2016), arXiv:1603.03457 [nucl-th]
- [54] U. Gürsoy, E. Kiritsis, L. Mazzanti, and F. Nitti, *JHEP* **05**, 033 (2009), arXiv:0812.0792 [hep-th]
- [55] R. Yaresko and B. Kämpfer, *Phys. Lett. B* **747**, 36 (2015), arXiv:1306.0214 [hep-ph]
- [56] R. Yaresko, J. Knaute, and B. Kämpfer, *Eur. Phys. J. C* **75**, 295 (2015), arXiv:1503.09065 [hep-ph]
- [57] S. S. Gubser and A. Nellore, *Phys. Rev. D* **78**, 086007 (2008), arXiv:0804.0434 [hep-th]
- [58] A. Peshier, B. Kämpfer, and G. Soff, *Phys. Rev. C* **61**, 045203 (2000), arXiv:hep-ph/9911474 [hep-ph]
- [59] A. Peshier, B. Kämpfer, and G. Soff, *Phys. Rev. D* **66**, 094003 (2002), arXiv:hep-ph/0206229 [hep-ph]
- [60] S. Plumari, W. M. Alberico, V. Greco, and C. Ratti, *Phys. Rev. D* **84**, 094004 (2011), arXiv:1103.5611 [hep-ph]
- [61] R. Bellwied, S. Borsanyi, Z. Fodor, S. D. Katz, A. Pasztor, C. Ratti, and K. K. Szabo, *Phys. Rev. D* **92**, 114505 (2015), arXiv:1507.04627 [hep-lat]